ELSEVIER

Thermochimica Acta 282/283 (1996) 69–80

thermochimica acta

Accommodation of the actual solid-state process in the kinetic model function. Part 2. Applicability of the empirical kinetic model function to diffusion-controlled reactions[1]

Nobuyoshi Koga [a,*], Jiri Malek [b]

[a] *Chemistry Laboratory, Faculty of School Education, Hiroshima University, 1-1 Kagamiyama 1-Chome, Higashi-Hiroshima 739, Japan*

[b] *Joint Laboratory of Solid State Chemistry, Academy of Sciences of the Czech Republic and University of Pardubice, Studentska 84, CR- 530 09 Pardubice, Czech Republic*

Abstract

The significance of the empirical kinetic model function for diffusion-controlled reactions is discussed in connection with the fractal nature of the reaction geometry and the macroscopic character of the thermoanalytical curves for solid-state reactions. The mathematical properties of such empirical kinetic model functions based on the geometrical fractal were investigated numerically in order to evaluate their practical usefulness as a possible diagnostic tool for distinguishing the most appropriate kinetic model function. The procedure of distinguishing the kinetic model function is extended, including such empirical kinetic model functions based on the geometrical fractal, and applied to the kinetic analysis of the thermal dehydroxylation of synthetic brochantite $Cu_4(OH)_6SO_4$.

Keywords: Brochantite; Decomposition; Fractal; Kinetic model function; Kinetics

1. Introduction

Although thermoanalytical (TA) data are of a macroscopic nature averaged over the assemblage of a sample, the experimentally resolved shape of TA curves has

* Corresponding author.

[1] Dedicated to Takeo Ozawa on the Occasion of his 65th Birthday.

SSDI 0040-6031(96)02822-5

been widely used as a possible source for the kinetic understanding of solid-state reactions [1]. The shape of the TA curve is characterized by the kinetic model function $f(\alpha)$ derived on the basis of the physico-geometric assumption of the reaction interface movement [2,3], because the solid-state reaction is especially characterized by the existence of a specialized zone of locally enhanced reactivity at the reactant/product contact, i.e., the reaction interface. The kinetics is further characterized assuming the Arrhenius-type temperature dependence of the rate constant, in which the apparent values of the activation energy E and preexponential factor A are the kinetic parameters. Accordingly, the TA curve is analyzed kinetically assuming the equation

$$\frac{d\alpha}{dt} = A \exp\left(-\frac{E}{RT}\right) f(\alpha) \tag{1}$$

where $\alpha, t, R,$ and T are the fractional reaction, time, gas constant and temperature, respectively.

Recently, it was shown [4,5] that, when the TA curves for the solid-state process under investigation cannot fully be described by the conventional kinetic model function $f(\alpha)$ because of the complexity of the reaction, the resultant kinetic parameters deviate from the true values as a simple mathematical consequence of Eq. (1). In this case, it can be useful to find an empirical function $h(\alpha)$ containing the smallest possible number of constants, so that there is some flexibility sufficient to describe the real process as closely as possible. In such a case, the kinetic model of heterogeneous reaction is assumed as a distorted case of the simpler homogeneous kinetics and then mathematically treated by multiplying by an accommodation function $a(\alpha)$ [6–8]

$$h(\alpha) = f(\alpha)a(\alpha) \tag{2}$$

Such an empirical kinetic model function has been proposed by Sestak and Berggren [9]

$$h(\alpha) = \alpha^m(1-\alpha)^n[-\ln(1-\alpha)]^r \tag{3}$$

It was believed that the Sestak–Berggren (SB) model function, containing as many as three exponents, is able to describe any TA curve [10]. Use of the nonintegral kinetic exponents in the conventional $f(\alpha)$ is also taken as one of the empirical kinetic models based on Eq. (2) [8]. Practically, empirical functions for a phase-boundary-controlled reaction and random nucleation and growth have been used, such as the reaction order (RO) and Johnson–Mehl–Avrami (JMA) models for characterizing solid-state reactions [8]. The mathematical properties of the empirical SB, RO and JMA models for applying practical kinetic analysis of TA curves were discussed comprehensively by Malek and Criado [11–14]. Although diffusion of the species is important in many solid-state reactions, an empirical kinetic model function for diffusion-controlled reactions has been missing in the formalism of TA kinetic analysis. Recently, Ozao and Ochiai discussed the kinetic model function for diffusion-controlled reactions on the

basis of the fractal nature of the reactant particle [15]. Adding the systematic understanding of the mathematical properties, the diffusion-controlled model with nonintegral kinetic exponent is probably included in the formalism of TA kinetic analysis as an empirical kinetic model function.

In the present paper, the significance of the empirical kinetic model function for the diffusion-controlled reaction is discussed in connection with the fractal nature of the reaction geometry and macroscopic character of the TA curves. The mathematical properties of such empirical kinetic model functions are investigated analytically in order to evaluate their practical usefulness. The practical procedure of distinguishing the kinetic model function is extended, including the empirical kinetic model function based on a diffusion-controlled reaction. A practical example of kinetic analysis is described for the thermal decomposition of synthetic brochantite $Cu_4(OH)_6SO_4$.

2. Theoretical

2.1. Empirical kinetic model function for diffusion-controlled reaction

As is the case with phase-boundary-controlled reactions, the conventional kinetic model function for the diffusion-controlled reactions is based on the geometrical constraints of reaction interface movement. Extension of the reaction geometry to nonintegral values is a possible way to formalize the empirical kinetic model function [7]. For example, the empirical kinetic model functions for the phase-boundary-controlled reaction R_n and random nucleation and growth A_m can easily be formalized with a nonintegral dimension [8].

Employing the nonintegral value of the dimension $1 \leq n \leq 3$, the following reaction is obtained

$$\frac{r}{r_0} = (1-\alpha)^{1/n} \tag{4}$$

where r and r_0 are the radii of the reactant particle at $t = 0$ and $t = t$. The nonintegral value n is described by reactions on a fractal domain, the hallmarks of which are anomalous orders and time-dependent reaction rate constants [16]. These anomalies stem from the nonrandomness of the reactant distributions. Among the practical examples of this fractal-like kinetics are chemical reactions in pores of membranes, excitation trapping in molecular aggregates, fusion in composite materials, and the processes in porous (Vycor) glass, assuming possible controversy about its pore topology [17].

For the diffusion-controlled reaction, Ozao and Ochiai [15] derived the following model functions with a nonintegral kinetic exponent by assuming the proportionality of the rate of volume shrinkage to the amount of diffused substance at time t and the

constant concentration gradient along the direction of diffusion

$$\text{(i)} \quad 1 \le n < 2 \qquad \frac{d\alpha}{dt} = \frac{K}{[1-(1-\alpha)^{2/n-1}]} \tag{5}$$

$$\text{(ii)} \quad n = 2 \qquad \frac{d\alpha}{dt} = \frac{K}{[-\ln(1-\alpha)]} \tag{6}$$

$$\text{(iii)} \quad 2 < n \le 3 \qquad \frac{d\alpha}{dt} = \frac{K}{[(1-\alpha)^{2/n-1}-1]} \tag{7}$$

where K is an apparent rate constant. Eqns. (5), (6) and (7) are taken as the kinetic rate equation for the diffusion-controlled reaction with geometrical fractal [15] corresponding to the conventional parabolic rate law [18], the two-dimensional diffusion law [19], and the Ginstling–Brounshtein law [20], respectively, when $n = 1, 2$ and 3.

In the practice of TA kinetics, it may be difficult to ascribe the nonintegral value of n determined from experimentally resolved shapes of TA curves to only a simple geometrical fractal, because of the macroscopic nature of the TA curves. Thus the kinetic rate equations for the diffusion–controlled reaction with a non-integral kinetic exponent are treated here as the empirical kinetic model function $h(\alpha)$ within the regime of Eq. (2). Table 1 lists the geometrical-fractal-based $h(\alpha)$ functions for the diffusion-

Table 1
The empirical kinetic model functions $h(\alpha)$, together with their integral forms $g(\alpha)$

Symbol	Range of exponent	$h(\alpha)$	$g(\alpha) = \int_0^\alpha \frac{d\alpha}{h(\alpha)}$
D_n	$1 \le n \le 2$	$\frac{1}{[1-(1-\alpha)^{2/n-1}]}$	$-\frac{n}{2}+\alpha+\frac{n}{2}(1-\alpha)^{2/n}$
	$n = 2$	$\frac{1}{[-\ln(1-\alpha)]}$	$\alpha+(1-\alpha)\ln(1-\alpha)$
	$2 < n \le 3$	$\frac{1}{[(1-\alpha)^{2/n-1}-1]}$	$\frac{n}{2}-\alpha-\frac{n}{2}(1-\alpha)^{2/n}$
R_n	$1 \le n \le 3$	$n(1-\alpha)^{1-1/n}$	$1-(1-\alpha)^{1/n}$
A_m	$0.5 \le n \le 4$	$m(1-\alpha)[-\ln(1-\alpha)]^{1-1/m}$	$[-\ln(1-\alpha)]^{1/m}$
RO(N)	–	$(1-\alpha)^N$	$\frac{1-(1-\alpha)^{1-N}}{1-N}$
JMA(M)	–	$M(1-\alpha)[-\ln(1-\alpha)]^{1-1/M}$	$[-\ln(1-\alpha)]^{1/M}$
SB(m, n)	–	$\alpha^m(1-\alpha)^n$	No analytical form

controlled D_n, phase-boundary-controlled R_n, and random nucleation and growth A_m models, together with those for the really empirical models RO(N), JMA(M) and SB(m, n).

2.2 *Mathematical properties of the empirical kinetic model function and its application*

Fig. 1 shows the dependence of the shape of the $h(\alpha)$ functions against α on the nonintegral value n. The $h(\alpha)$ curves are concave and have maxima at $\alpha_M = 0$, as is the case with conventional $f(\alpha)$ for diffusion-controlled reactions [13]. The kinetic parameters are calculated from a single nonisothermal TA curve by using the logarithmic form of Eq. (1) [21]

$$\ln\left[\frac{(d\alpha/dT)}{h(\alpha)}\right] = \ln\left(\frac{A}{\phi}\right) - \frac{E}{RT} \tag{8}$$

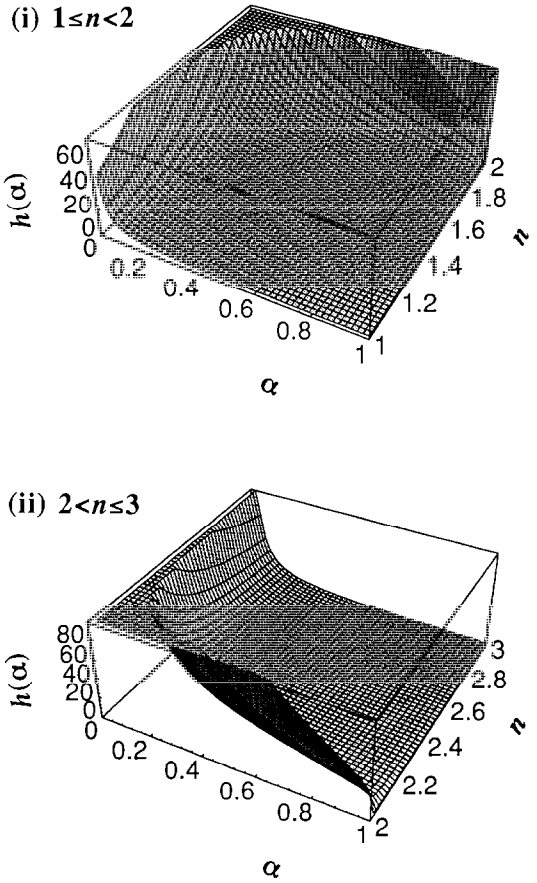

Fig. 1. Dependence of $h(\alpha)$ on α and n for diffusion-controlled reactions.

where ϕ is the heating rate. Because the $h(\alpha)$ function participates in Eq. (8) as a logarithmic term, it seems less meaningful to discuss the slight variation of the nonintegral value of n in the single-run method. In addition, such ambiguity in determining $h(\alpha)$ affects the apparent values of both the Arrhenius parameters, E and A, as a result of the mutual dependence of the apparent kinetic parameters [22].

The above problem of calculating the kinetic parameters is eliminated if the characteristic value of activation energy for the process is already known. Then the following formalism is obtained from Eq. (1) [11, 13, 23]

$$y(\alpha) = \frac{\mathrm{d}\alpha}{\mathrm{d}\theta} = \frac{\mathrm{d}\alpha}{\mathrm{d}t}\exp\left(\frac{E}{RT}\right) = Ah(\alpha) \tag{9}$$

where θ is the generalized time introduced by Ozawa in 1965 [24–26]. Both sides of Eq. (9) being a function of α, the process is characterized by the original shape of $h(\alpha)$. Through plots of $y(\alpha)$ against various $h(\alpha)$, the most appropriate $h(\alpha)$ represents the best linearity and the value of A is calculated from the slope [27].

It was shown [7, 11, 13, 28, 29] that the multiplied function of $h(\alpha)$ and $g(\alpha)$ is a useful diagnostic tool for determining the most appropriate kinetic model function, in which all the functions have a maximum at a characteristic value of α_p. The function $h(\alpha)g(\alpha)$ appears in the kinetic equation as follows

$$\frac{\mathrm{d}\alpha}{\mathrm{d}t} = \left[\frac{\phi}{T\pi(x)}\right]h(\alpha)g(\alpha) \tag{10}$$

with

$$g(\alpha) = \int_0^{\alpha}\frac{\mathrm{d}\alpha}{h(\alpha)} = \frac{AE}{\phi R}\exp(-x)\left[\frac{\pi(x)}{x}\right] \tag{11}$$

where $\pi(x)$ is an approximation of exponential integration and $x = E/RT$. Fig. 2 shows the dependence of the shape of the $h(\alpha)g(\alpha)$ functions for diffusion-controlled reactions against α on the nonintegral value n. The functions have a maximum at $\alpha_p > 0.776$. The value of α_p is characteristic for the $h(\alpha)$ of a diffusion-controlled model, different from that in other empirical $h(\alpha)$ functions [7, 13]. After rearrangement of Eq. (10), the $z(\alpha)$ function is defined as

$$z(\alpha) = h(\alpha)g(\alpha) = \pi(x)\frac{\mathrm{d}\alpha}{\mathrm{d}t}\frac{T}{\phi} \tag{12}$$

Differentiation of Eq. (10) gives

$$\left(\frac{\mathrm{d}^2\alpha}{\mathrm{d}t^2}\right) = \left[\frac{\phi}{T\pi(x)}\right]^2 h(\alpha)g(\alpha)\left[h'(\alpha)g(\alpha) + x\pi(x)\right] \tag{13}$$

By setting Eq. (13) equal to zero, the mathematical condition for the TA peak is obtained

$$-h'(\alpha_p)g(\alpha_p) = x_p\pi(x_p) \tag{14}$$

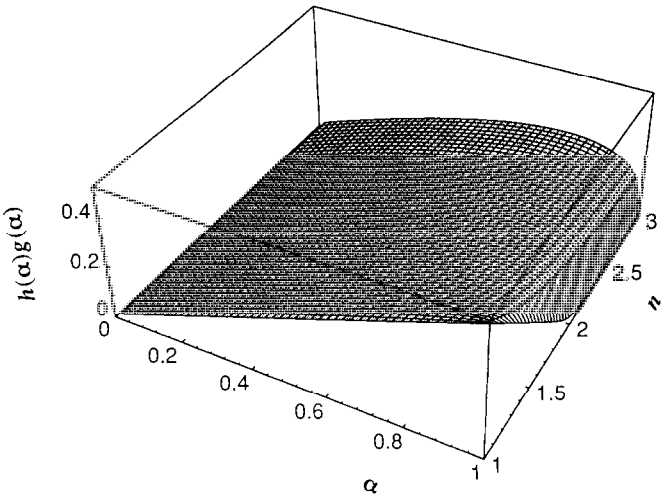

Fig. 2. Dependence of $h(\alpha)g(\alpha)$ on α and n for diffusion-controlled reactions.

When x_p is infinite, Eq. (14) is written as

$$-h'(\alpha_p^{\infty})g(\alpha_p^{\infty}) = \lim_{x_p \to \infty} [x_p \pi(x_p)] = 1 \tag{15}$$

where α_p^{∞} is the α_p at $x_p \to \infty$. Using Eq. (15), the value of α_p^{∞} is obtained numerically for the function $h(\alpha)g(\alpha)$ of the diffusion-controlled model. Fig. 3 shows the dependence of α_p^{∞} on the nonintegral value n. The α_p^{∞} increases from 0.774 to 1.0 on decreasing the n value from 3.0 to 1.0.

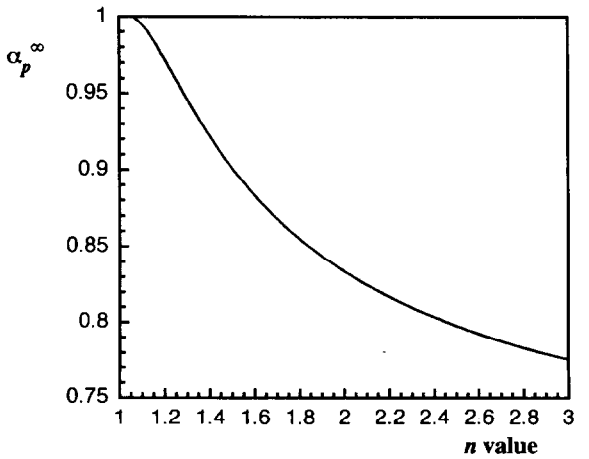

Fig. 3. Dependence of α_p^{∞} of $h(\alpha)g(\alpha)$ on the kinetic exponent n for diffusion-controlled reactions.

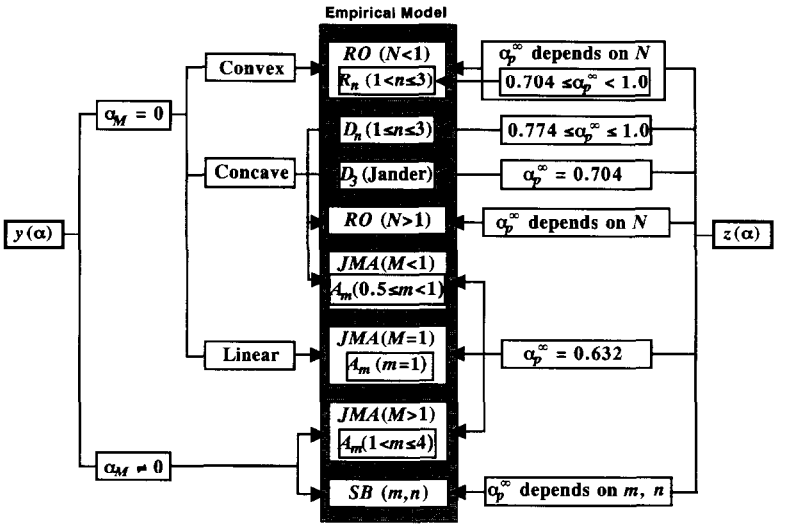

Fig. 4. Schematic diagram of the kinetic model determination using the $y(\alpha)$ and $z(\alpha)$ functions.

It is apparent that the empirical D_n model is characterized as concave, having the maximum at $\alpha_M = 0$ in the $y(\alpha)$ function and the maximum within $0.774 \leq \alpha_p^{\infty} \leq 1.0$ in the $z(\alpha)$ function. Fig. 4 shows schematically the empirical kinetic model determination by means of $y(\alpha)$ and $z(\alpha)$ functions. By adding the empirical model functions based on the geometrical fractal, the empirical RO(N) and JMA(M) functions can be related to the conventional kinetic model functions $f(\alpha)$ with integral kinetic exponents. However, the SB (m, n) function really has an empirical character, which in turn makes it possible to describe various types of shape of TA curves fulfilling $\alpha_M \neq 0$.

3. Experimental

Precipitates of basic copper(II) sulfate were obtained at 25°C by adding 0.1 M NaOH solution dropwise at a rate of 1.0 ml min^{-1} with stirring to 100 ml 0.1 M $CuSO_4$ solution until the pH of the resulting solution was equal to 8.0 [30,31]. The precipitates, dried in air and ground in a mortar, were characterized by means of X-ray powder diffractometry, FT–IR spectroscopy and thermogravimetry (TG) and identified as corresponding to the mineral brochantite $Cu_4(OH)_6SO_4$.

10.0 mg of the sample, sieved to the $-170+200$ mesh fraction, was weighed into a platinum crucible 5 mm in diameter and 2.5 mm in depth. TG–DTG curves were recorded simultaneously at various heating rates $1.0 \leq \phi \leq 10.0$ K min^{-1} in a flow of N_2 at a rate of 30 ml min^{-1}, using a Shimadzu TGA-50 apparatus. It is known that the thermal dehydroxylation proceeds by the following two-step reactions [30–33]

$$Cu_4(OH)_6SO_4 \rightarrow Cu_4O(OH)_4SO_4 + H_2O \quad (16)$$

$$Cu_4O(OH)_4SO_4 \rightarrow Cu_4O_3SO_4 + 2H_2O \quad (17)$$

The intermediate compound $Cu_4O(OH)_4SO_4$ was prepared by heating 10.0 mg of the sample at 255°C for 15 h in the above TG apparatus. In order to obtain the TG curves for the second reaction, the product was cooled down to room temperature and again heated up to 500°C under conditions identical with the above TG measurements. TG curves for the first reaction at various heating rates were obtained by subtracting the TG curve for the second reaction from that for the overall dehydroxylation. The respective reaction steps of the dehydroxylation were analyzed kinetically along the diagram shown in Fig. 4.

4. Results and discussion

Fig. 5 shows the typical TG–DTG curves obtained at a heating rate of 10 K min^{-1}. The respective reaction steps of the thermal dehydroxylation are not clearly separated and are only recognized by the anomalies in the DTG curve. Typical plots of α against T for the respective reaction steps obtained by the experimental treatment described above are shown in Fig. 6. The mass loss due to the respective reactions corresponds quantitatively to Eqs. (16) and (17). The apparent activation energies E at various α were calculated using the Friedman method [34] by plotting $\ln(d\alpha/dt)$ against T^{-1} at a restricted α

$$\ln\left(\frac{d\alpha}{dt}\right) = \ln[Af(\alpha)] - \frac{E}{RT} \tag{18}$$

The constancy of E values among different α is the prerequisite for the subsequent kinetic approach based on Eq. (1), which in turn provides the criterion for the appropriate kinetic analysis [22,35]. The constant E values of 158.0 ± 1.3 and

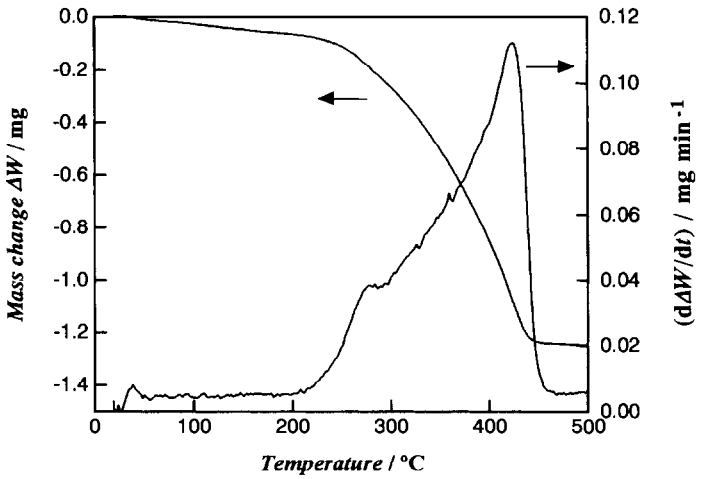

Fig. 5. Typical TG–DTG curves for the thermal dehydroxylation of synthetic brochantite at a heating rate of 10 K min^{-1}.

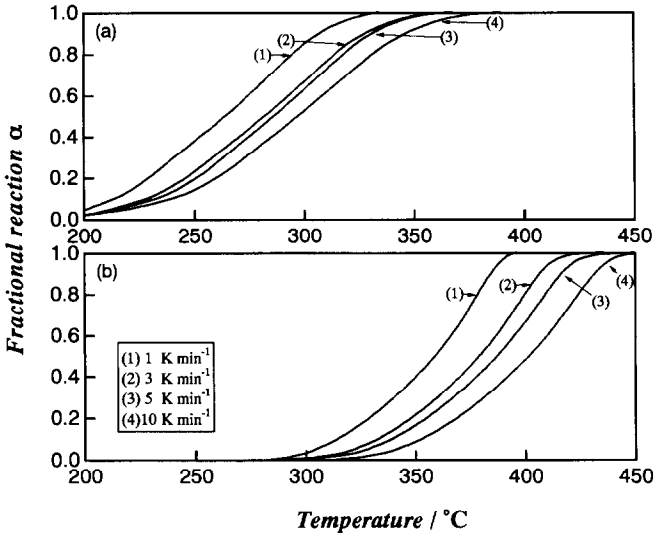

Fig. 6. Typical plots of α against T for the thermal dehydroxylation of synthetic brochantite: (a) $Cu_4(OH)_6SO_4 \rightarrow Cu_4O(OH)_4SO_4 + H_2O$; (b) $Cu_4O(OH)_4SO_4 \rightarrow Cu_4O_3SO_4 + 2H_2O$.

193.1 ± 0.9 kJ mol^{-1} were obtained for the first and second reactions in the range $0.2 \leq \alpha \leq 0.8$ and $0.1 \leq \alpha \leq 0.9$, respectively.

According to Eq. (9), the kinetic rate data at various heating rates were extrapolated to infinite temperature obtaining a plot of $y(\alpha)$ against α [35]. Fig. 7 shows the comparison of the $y(\alpha)$ vs. α plot between the respective reactions. Agreement of the rate data with a particular kinetic model function was investigated through plots of the various $h(\alpha)$ listed in Table 1 against $y(\alpha)$. The A_m and D_n laws were selected as the possible kinetic model functions for both reactions. Table 2 lists the appropriate kinetic exponents m and n in the A_m and D_n functions, together with the preexponential factors. It is difficult to distinguish the most appropriate $h(\alpha)$ from only the linearity of $h(\alpha)$ against $y(\alpha)$.

In order to determine the most appropriate kinetic model function, the plots of $z(\alpha)$ against α were obtained according to Eq. (12) using the approximation [36]

$$\pi(x) = \frac{x^3 + 18x^2 + 88x + 96}{x^4 + 20x^3 + 120x^2 + 240x + 120} \tag{19}$$

The $z(\alpha)$ against α plots for the respective reactions are also shown in Fig. 7. The plots of $z(\alpha)$ against α have maxima at $\alpha_p^\infty = 0.64$ and $\alpha_p^\infty = 0.80$ for the first and second reactions, respectively. The value $\alpha_p^\infty = 0.64$ for the first reaction apparently indicates possible agreement with the A_m-type model. The $A_{0.5}$ function is thus selected as the most appropriate model function for the first reaction, see Table 2. The second reaction with $\alpha_p^\infty = 0.80$ is identified as obeying the D_n law and the exponent $n = 2.6$ is satisfied by the relation between α_p^∞ and n, see Fig. 4.

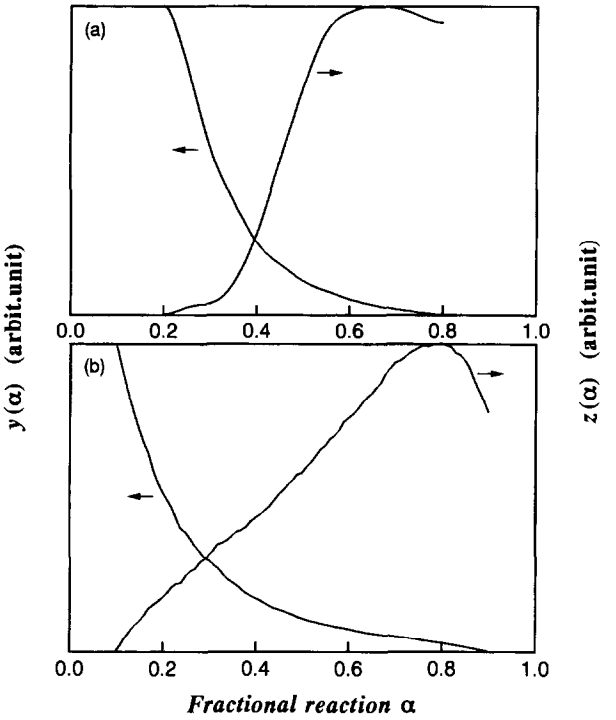

Fig. 7. Plots of $y(\alpha)$ and $z(\alpha)$ against α for the thermal dehydroxylation of synthetic brochantite: (a) $Cu_4(OH)_6SO_4 \rightarrow Cu_4O(OH)_4SO_4 + H_2O$; (b) $Cu_4O(OH)_4SO_4 \rightarrow Cu_4O_3SO_4 + 2H_2O$.

Table 2
The empirical kinetic model function $h(\alpha)$ and the preexponential factor A for the thermal dehydroxylation of synthetic brochantite determined by plotting $h(\alpha)$ against $y(\alpha)$

Reaction	$h(\alpha)$	Exponent	A/s^{-1}	γ^a
$Cu_4(OH)_6SO_4$	A_m	$m = 0.5$	1.79×10^{12}	0.9926
$\rightarrow Cu_4O(OH)_4SO_4 + H_2O$	D_n	$n = 1.0$	8.29×10^{11}	0.9884
$Cu_4O(OH)_4SO_4$	A_m	$m = 0.6$	4.99×10^{12}	0.9958
$\rightarrow Cu_4SO_4 + 2H_2O$	D_n	$n = 2.6$	3.28×10^{11}	0.9971

[a] Correlation coefficient of the linear regression analysis of the $h(\alpha)$ against $y(\alpha)$ plot.

Although the kinetic model determination by the combination of $y(\alpha)$ and $z(\alpha)$ is especially suitable for the nucleation-growth processes, having the capability of distinguishing SB models from JMA models as complicated nucleation-growth processes [37], the present kinetic analysis exemplifies the successful application of the method to the thermal decomposition of solids. On applying the method to the thermal decomposition of solids, the RO and/or the present D_n models play an important role

in accommodating the actual reaction process in the kinetic model function as an extended interpretation of the phase- boundary-controlled and/or diffusion-controlled model. In the scheme of the $y(\alpha)$ and $z(\alpha)$ functions, the empirical D_n model can be distinguished successfully from the RO, JMA and SB models.

References

[1] J. Sestak, Thermophysical Properties of Solids, Elsevier, Amsterdam, 1984.
[2] S.F. Hulbert, J. Brt. Ceram. Soc., 6 (1969) 11.
[3] M.E. Brown, D. Dollimore and A.K. Galwey, Reactions in the Solid State, Elsevier, Amsterdam, 1980.
[4] N. Koga, J. Sestak and J. Malek, Thermochim. Acta, 188 (1991) 333.
[5] N. Koga and J. Sestak, J. Therm. Anal., 37 (1991) 1103.
[6] J. Sestak, J. Therm. Anal., 36 (1990) 1977.
[7] N. Koga, J. Malek, J. Sestak and H. Tanaka, Netsu Sokutei (Calor. Therm. Anal.), 20 (1993) 210.
[8] N. Koga and H. Tanaka, J. Therm. Anal., 41 (1994) 455.
[9] J. Sestak and G. Berggren, Thermochim. Acta, 3 (1971) 1.
[10] J. Sestak, J. Therm. Anal., 16 (1979) 503; 33 (1988) 1263.
[11] J. Malek, Thermochim. Acta, 138 (1989) 377.
[12] J. Malek and J. Criado, Thermochim. Acta, 164 (1990) 199.
[13] J. Malek, Thermochim. Acta, 200 (1992) 257.
[14] J. Malek and J. Criado, Thermochim. Acta, 203 (1992) 25.
[15] R. Ozao and M. Ochiai, J. Ceram. Soc. Jpn., 101 (1993) 263.
[16] R. Kopelman, Science, 241 (1988) 1620.
[17] J. Prasad and R. Kopelman, Phys. Rev. Lett., 56 (1986) 1742
[18] W. Jander, I.Z. Anorg. Chem., 163 (1927) 1.
[19] J.B. Holt, J.B. Cutler and M.E. Wadsworth, J. Am. Ceram. Soc., 45 (1962) 133.
[20] A.M. Ginstling and B.I. Brounshtein, J. Appl. Chem. USSR, English Trans., 23 (1950) 1327.
[21] B.N. Achar, G.W. Brindley and J.H. Sharp, Proc. 1st. Clay Conf., Jerusalem, 1966, p. 67.
[22] N. Koga, Thermochim. Acta, 244 (1994) 1.
[23] T. Ozawa, J. Therm. Anal., 2 (1970) 301; 31 (1986) 547.
[24] T. Ozawa, Bull. Chem. Soc. Jpn., 38 (1965) 1881.
[25] T. Ozawa, J. Therm. Anal., 2 (1970) 301.
[26] T. Ozawa, Thermochim. Acta, 100 (1986) 109.
[27] N. Koga and H. Tanaka, Thermochim. Acta, 224 (1993) 141.
[28] J. Malek, J. Sestek, F. Rouquerol, J. Rouquerol, J.M. Criado and A. Ortega, J. Therm. Anal., 38 (1992) 71.
[29] J. Sestak and J. Malek, Solid State Ionics, 63–65 (1993) 245.
[30] H. Tanaka and N. Koga, Thermochim. Acta, 133 (1988) 221; J. Chem. Educ., 67 (1990) 612.
[31] H. Tanaka, M. Kawano and N. Koga, Thermochim. Acta, 182 (1991) 281.
[32] P. Ramamurthy and E.A. Secco, Can J. Chem., 48 (1970) 3510.
[33] E.A. Secco, Can. J. Chem., 66 (1988) 337.
[34] H.L. Friedman, J. Polym. Sci., C6 (1964) 183.
[35] N. Koga, Thermochim. Acta, 258 (1995) 145.
[36] G.I. Senum and R.T. Yang, J. Therm. Anal., 11 (1977) 445.
[37] J. Malek, Thermochim. Acta, 267 (1995) 61.